



**HAL**  
open science

## Texture and material classification with multi-scale ternary and septenary patterns

E. Rachdi, I. El Khadiri, Youssef El Merabet, Y. Rhazi, Cyril Meurie

► **To cite this version:**

E. Rachdi, I. El Khadiri, Youssef El Merabet, Y. Rhazi, Cyril Meurie. Texture and material classification with multi-scale ternary and septenary patterns. *Journal of King Saud University - Computer and Information Sciences*, 2022, 35 (1), pp.405-415. 10.1016/j.jksuci.2022.12.009 . hal-04522078

**HAL Id: hal-04522078**

**<https://univ-eiffel.hal.science/hal-04522078>**

Submitted on 26 Mar 2024

**HAL** is a multi-disciplinary open access archive for the deposit and dissemination of scientific research documents, whether they are published or not. The documents may come from teaching and research institutions in France or abroad, or from public or private research centers.

L'archive ouverte pluridisciplinaire **HAL**, est destinée au dépôt et à la diffusion de documents scientifiques de niveau recherche, publiés ou non, émanant des établissements d'enseignement et de recherche français ou étrangers, des laboratoires publics ou privés.

HOSTED BY



ELSEVIER

Contents lists available at ScienceDirect

Journal of King Saud University –  
Computer and Information Sciencesjournal homepage: [www.sciencedirect.com](http://www.sciencedirect.com)

## Texture and material classification with multi-scale ternary and septenary patterns

E. Rachdi<sup>a</sup>, I. El khadiri<sup>a,d</sup>, Y. El merabet<sup>a,\*</sup>, Y. Rhazi<sup>b</sup>, C. Meurie<sup>c</sup><sup>a</sup> Laboratoire SETIME, Département de Physique, Faculté des Sciences, Université Ibn Tofail, BP 133, Kénitra 14000, Morocco<sup>b</sup> Electrical Engineering Department, Faculty of Sciences and Technology, Beni-Mel lal, Morocco<sup>c</sup> Univ Gustave Eiffel, COSYS-LEOST, F-59650 Vil leneuve d'Ascq, France<sup>d</sup> The Department of Algorithms and Their Applications, Eötvös Loránd University, Budapest, Hungary

## ARTICLE INFO

## Article history:

Received 16 August 2022

Revised 19 November 2022

Accepted 14 December 2022

Available online 22 December 2022

## Keywords:

Texture classification

Texture descriptors

LBP

Feature extraction

Directional topologies

## ABSTRACT

This paper ideates, inspired by LBP and its variants, a novel local feature extraction operator for texture classification, referred to as Multi-scale Ternary and Septenary Pattern (MTSP). MTSP is a histogram-based feature representation that is composed of two single-scale STP and SSP (single-scale ternary and septenary patterns, respectively) encoders designed according to a novel set theory based pattern encoding scheme that integrates the concepts of both LQP's and LTP's operators. The essence of STP and SSP is to compute several virtual pixels based on various local and global image statistics and progressively encode interactions between local and non-local pixels by examining the directional information and differential excitation according to relationships between adjacent pixels rearranged in a variety of spatial arrangements. Unlike various parametric state-of-the-art texture operators that perform thresholding based on static thresholds, MTSP incorporates dynamic thresholds estimated automatically. MTSP descriptor has good ability as faithfully as possible to capture more detailed image information via complementary texture information generated from the fusion of both STP and SSP encoders. Experimental results show that MTSP ensures reliable performance stability over ten texture datasets and against several recent representative methods. In addition, the performance of MTSP is further proved statistically via the Wilcoxon signed rank test demonstrating thus that MTSP is a good candidate for texture modeling.

© 2022 The Author(s). Published by Elsevier B.V. on behalf of King Saud University. This is an open access article under the CC BY-NC-ND license (<http://creativecommons.org/licenses/by-nc-nd/4.0/>).

## 1. Introduction

In the field of texture analysis, the classification of textures is increasingly seen as a serious problem. It plays a major role in a wide range of applications, such as face presentation attack detection (Li et al., 2022), image classification (Fernandez et al., 2011), writer identification (Bahram, 2022), image retrieval (Banerjee et al., 2018), object and scene recognition (Torrallba et al., 2008), pedestrian detection (Zheng et al., 2017), gender classification (Hadid et al., 2015), facial classification (Chakraborty et al., 2018), etc. However, in the real world, textures vary in scale,

illumination, rotation and affine varieties as imaging conditions changes. In texture analysis, extracting powerful features for texture categorization is still a gauntlet. Over the years, numerous advanced approaches were developed in the literature with excellent surveys given in Liu et al. (2019). Several traditional feature extraction approaches have been proposed such as, occurrence matrix-based approaches (Davis, 1981), filter-based techniques such as wavelet (Porter and Canagarajah, 1997, April.), Gabor (Manjunath and Ma, 1996) and Gaussian Markov random fields (Cohen et al., 1991), fractal analysis-based methods (Xu et al., 2010), texton dictionary-based methods (Varma and Zisserman, 2008), etc. Over the past decades, local feature extraction techniques have been designed and have demonstrated great success in the field of texture analysis. The primary benefits of these texture descriptors come from the fact that they only depend on a relatively modest amount of training data and their straightforward design (Bhattacharjee and Roy, 2021).

Among the local texture descriptors, LBP (local binary patterns) (Ojala et al., 1996), has become one of the most remarkable and

\* Corresponding author.

E-mail address: [youssef.elmerabet@uit.ac.ma](mailto:youssef.elmerabet@uit.ac.ma) (Y. El merabet).

Peer review under responsibility of King Saud University.



Production and hosting by Elsevier

attractive texture descriptor and has attracted greater interest for more than a decade. LBP is highly regarded by scientists due to its distinctive merits including ease to train with a small amount of data, implementation simplicity, suitability to solve high-class texture problems with real-time applications due to its relative fast calculation, invariability to monotonic illumination variations, etc. (Rachdi et al., 2020). Despite these advantages, LBP also has many limitations (Ruichek, 2018) such as: (1) It is sensitive to noise since it is based only on the comparison between local pixels; (2) It disregards the image's comprehensive spatial information in favor of local texture elements; (3) It is not invariant to image rotation, etc. Several attempts have been made to overcome the shortcomings of LBP, and as a result, many modifications and extensions built on LBP have been designed in recent years. Guo et al. (2012), Guo et al. (2010), Fernandez et al. (2011), Kas et al. (2018). The authors in El Idrissi et al. (2020) provided thorough tests evaluating the performance of various state-of-the-art texture operators in palm-print and face recognition problems, respectively. To overcome the sensitivity of LBP to central pixel noise, local ternary pattern (LTP) (Tan and Triggs, 2010) has been introduced. In LTP, by assigning a threshold to the central pixel, the descriptor is quantized into three levels (-1, 0, and 1) and decomposed into two upper and lower descriptors. In El-khadiri et al. (2018), the authors presented local directional ternary pattern (LDTP) operator that encodes both directional and contrast informations using the concepts of LDP and LTP operators. More recently, Shih et al. (2020) designed synchronized rotation local ternary pattern (SRLTP) operator for image classification. SRLTP operator consists in improving the LTP operator by using an additional procedure on the extracted upper and lower LTPs which are henceforth encoded to a uniform and rotation invariant patterns histograms, respectively. In Tuncer and Dogan (2020), multi kernel based local binary pattern (MKLBP) descriptor is proposed for texture classification. The construction process of MKLBP integrates ternary, quaternary and signum feature extraction operators into the same encoding scheme. The authors in Al Saidi et al. (2022) proposed corner rhombus shape LBP (CRSLBP) descriptor for texture classification. As an extension of LBP operator, CRSLBP in addition to using a single parameter (radius) and the selected even block, it takes into account magnitude and sign information, to threshold four center pixels. This permit to encode relationships between the centers and the neighbor of centers as well as neighbors. In Zheng et al. (2022), Zheng et al. proposed circumferential local ternary pattern (CLTP) for anti-counterfeiting pattern identification. CLTP classify each triplet of pixels composed by two circumferential adjacent pixels and the central pixels in each  $3 \times 3$  square neighborhood into falling, rising and stable structures. The local information is encoded using the LTP's concept.

LBP-like techniques have dominated the best position of local feature algorithms for more than a decade. The need to develop a discriminative local image feature operator no longer needs approval and the emergence of new local hand-crafted methods in pattern recognition is still ongoing, e.g., center Lop-Sided Local Binary Patterns (CLS-LBP) (Dawood et al., 2022), quaternionic local angular binary pattern (QLABP) (Lan et al., 2019), local concave-and-convex micro-structure (LCCMSP) (Ruichek, 2018), multi-direction local binary pattern (MDLBP) (Liu et al., 2019), scale-selective and noise-robust extended local binary pattern (SNELBP) (Luo et al., 2022), multi level directional cross binary patterns (MLD-CBP) (Kas et al., 2020), petersen graph multi-orientation based multi-scale ternary pattern (PGMO-MSTP) (El Khadiri et al., 2021), oriented star sampling structure based multi-scale ternary pattern (O3S-MTP) (El khadiri et al., 2020), orthogonal difference-local binary pattern (OD-LBP) (Karanwal and Diwakar, 2021), directional neighborhood topologies based multi-scale quinary pattern (DNT-MQP) (Rachdi et al., 2020), quaternionic extended

local binary pattern (QxLBP) (Song et al., 2021), adaptively binarizing magnitude vector (ABMV) (Hu et al., 2022) and so on.

Handcrafted texture methods appear to be progressively replaced by CNN-based methods (Shu, 2022). However, the main criticism of CNN come from the observation that they requires expensive model learning on massive data to achieve high recognition accuracy, but at the expense of computation time that is very expensive compared to hand-crafted features. In 2017, Liu et al. (2017) evaluated large number of LBP variants and compared them to some deep texture methods. Their findings revealed that the best overall performance is obtained by their designed handcrafted descriptor. Yang et al. (2020) have shown that handcrafted methods are efficient based directly on human knowledge. Song et al. (2020) indicate that basic deep features lack some robustness to rotation and illumination changes, while their designed handcrafted texture descriptor have great advantages in this regard. On the other side, Huang et al. in Huang and Yin (2017) have demonstrated how a structured and reliable local descriptor can enhance deep learning's remarkable capacity to extract more discriminating features. Similar comments are highlighted in Karczmarek et al. (2017)).

In summary and in light of above findings, the need to design a robust handcrafted texture method with high discriminant power is no longer to be proved. On the other hand, despite the promising results of LBP and its extensions and modifications, still an alternative solution to strengthen their power of discrimination for better representation of salient local texture structure, is crucial. In this paper, to better address the limitations of local feature descriptors and in particular LBP-like algorithms and thus to further improve their performance while keeping their easiness and efficiency, we develop a computationally and conceptually simple yet powerful local texture descriptor, named multi-scale ternary and septenary patterns (MTSP), for image texture understanding and analysis. The idea behind MTSP method is to compute the feature representation using different neighbourhood topologies, in order to catch comprehensive spatial information from neighbouring pixels in multiple direction and blocks and also to characterize the spatial relationship and the appearance of a given pixel intensity. The MTSP operator is obtained as being a concatenation of two single scale descriptors STP (Single-scale Ternary Pattern) and SSP (Single-scale Septenary Pattern) where information extraction is carried out according to a compact encoding scheme based on set theory integrating both the concepts of LQP and LTP-like texture methods to provide more discriminative texture information. MTSP has the advantage of being training free and conceptually much easier to implement. Furthermore, let us note that the major advantage of the proposed MTSP model lies in its flexibility given by its adaptive thresholding mechanism that uses dynamic thresholds estimated automatically inside each local compact neighborhood. In this context, the four main contributions of this paper are as follows:

- Two single scale feature descriptors called single-scale ternary pattern (STP) and single-scale septenary pattern (SSP) are designed based on novel set theory based pattern encoding scheme. It extends the concepts of both LTP and LQP operators using multiple oriented blocks and directions based neighborhood topologies which are more suitable for texture modeling against vast number of state-of-the-art methods.
- Both single-scale STP and SSP operators are combined together into a single vector feature construct the distinctive MTSP method which ought to be more effective and more reliable.
- Unlike vast number of existing parametric methods which use static thresholds, the creation process of MTSP incorporates dynamic thresholds which are estimated via an automatic mechanism.

- We provide thorough comparison on ten challenging datasets and prove that MTSP shows superior of competitive performance against recent powerful existing texture methods.

The structure of the rest of this paper is as follows. Section 2 briefly presents some typical state-of-the-art texture methods. Section 3 describes in detail the proposed MTSP texture descriptor. Comprehensive experiments and comparative evaluation are given in Section 4. Section 5 presents the implementation details to compare the processing time of all evaluated methods. Section 6 summarizes the study and presents some future research directions.

## 2. Background: LBP, LTP and LQP

### 2.1. Basic Local binary pattern (LBP)

The popular texture operator LBP, which demonstrated to be a very effective and computationally simple texture descriptor for monochromatic images, was introduced by Ojala et al. (1996). For each pixel in the image  $\mathbf{I}$  of size  $M \times N$ , a LBP value is computed by comparing its intensity value with those of its surrounding neighbors in each  $3 \times 3$  grayscale image patch. Formally, given a central pixel  $\mathbf{I}_c$  in a  $3 \times 3$  square neighborhood, its LBP label is generated based on the kernel function  $LBP(\cdot)$  (cf. Eq. (1)).

$$LBP(\mathbf{I}_c) = \sum_{p=0}^{P-1} \vartheta(\mathbf{I}_p - \mathbf{I}_c) \times 2^p \quad (1)$$

where  $\mathbf{I}_p (p \in \{0, 1, \dots, P-1\})$  denotes the  $p^{th}$  surrounding pixel,  $P (P=8)$  is the number of surrounding pixels.  $\vartheta$  is defined as follows (cf. Eq. (2)):

$$\vartheta(\mathbf{a}) = \begin{cases} 1 & \text{if } \mathbf{a} \geq 0 \\ 0 & \text{otherwise} \end{cases} \quad (2)$$

### 2.2. Local Ternary pattern (LTP)

The authors in Tan and Triggs (2010) extended the traditional LBP to three-value encoding scheme referred to as LTP, in which the two conventional binary codes (0 and 1) are extended to ternary codes (-1, 0 and 1). LTP uses a constant threshold value  $\tau$  specified by the user to compare the central pixel with its neighbouring pixels. The 3-valued function  $\varphi(\cdot)$  is given as follows (cf. Eq. (3)):

$$\varphi(\mathbf{I}_p, \mathbf{I}_c, \tau) = \begin{cases} +1 & \text{if } \mathbf{I}_p \geq \mathbf{I}_c + \tau \\ 0 & \text{if } |(\mathbf{I}_p - \mathbf{I}_c)| < \tau \\ -1 & \text{if } \mathbf{I}_p \leq \mathbf{I}_c - \tau \end{cases} \quad (3)$$

Consequently, by using the function  $\varphi(\cdot)$ , local ternary patterns upper ( $LTP_U$ ) and local ternary patterns lower ( $LTP_L$ ) are coded as following (cf. Eqs. (4) and (5)):

$$LTP_L(\mathbf{I}_c) = \sum_{p=0}^7 2^p \vartheta(\mathbf{I}_c - \mathbf{I}_p - \tau) \quad (4)$$

$$LTP_U(\mathbf{I}_c) = \sum_{p=0}^7 2^p \vartheta(\mathbf{I}_p - \mathbf{I}_c - \tau) \quad (5)$$

The final LTP code generated for each pixel of the image, is the combination of the two  $LTP_U$  and  $LTP_L$  texture features.

### 2.3. Local quinary patterns (LQP)

Loris Nanni et al. (2010), inspired by LTP, have extended LBP method to five-value encoding technique referred to as LQP in which the two conventional binary codes (0 and 1) are extended

to quinary codes (-2, -1, 0, 1 and 2) based on two constant thresholds  $\tau_1$  and  $\tau_2$ . The 5-valued function  $v(\cdot)$  is given as follows (cf. Eq. (6)):

$$v(\mathbf{I}_p, \mathbf{I}_c, \tau_1, \tau_2) = \begin{cases} +2 & \text{if } \mathbf{I}_p \geq \mathbf{I}_c + \tau_2 \\ +1 & \text{if } \mathbf{I}_c + \tau_1 \leq \mathbf{I}_p < \mathbf{I}_c + \tau_2 \\ 0 & \text{if } \mathbf{I}_c - \tau_1 \leq \mathbf{I}_p < \mathbf{I}_c + \tau_1 \\ -1 & \text{if } \mathbf{I}_c - \tau_2 \leq \mathbf{I}_p < \mathbf{I}_c - \tau_1 \\ -2 & \text{otherwise} \end{cases} \quad (6)$$

where  $\tau_1$  and  $\tau_2$  are two constant thresholds.

Subsequently, the obtained LQP is split into four binary patterns using the  $b_c(\mathbf{x})$  function and  $c \in \{2, 1, 0, -1, -2\}$ . Finally, the histograms produced from the binary patterns are concatenated.

$$b_c(\mathbf{x}) = \begin{cases} 1 & \text{if } \mathbf{x} == c \\ 0 & \text{otherwise} \end{cases} \quad (7)$$

## 3. Multi-scale Ternary and Septenary Patterns (MTSP)

MTSP is derived from the relationship between the local neighboring pixels and their central pixel in each  $3 \times 3$  patch by combining the concepts of LQP- and LTP-like texture methods in the same compact encoding strategy, increasing the texture modeling's accuracy, which leads to more hopeful outcomes. The essence of MTSP is to carry out pixels sampling and pattern encoding in the most relevant directions present in local microstructures. The construction process of MTSP descriptor that we propose, involves the following steps:

### 3.1. Pattern sampling

It is worth mentioning that MTSP operator takes into account a unit distance radius as nearest surrounding pixels keeps more discriminative information for local texture modeling retaining thus lower feature size and computational cost. Thus, the whole  $3 \times 3$  square neighborhood is chosen as spatial micro-structure to build the MTSP descriptor which conveys valuable information between the adjacent neighbouring pixels. Given a central pixel  $\mathbf{I}_c$  and its 8 surrounding pixels  $\{\mathbf{I}_0, \mathbf{I}_1, \dots, \mathbf{I}_7\}$  and based on the commonly used assumption that a texture information is derived from local spatial fluctuations in pixel intensities and orientation, MTSP considers multiple oriented blocks and directions based neighborhood topologies to encode the relationships and interactions between neighbouring pixels. As illustrated in Figs. 1 and 2, the pixels are sampled around the central pixel in a variety of spatial arrangements according to their angular position to catch more comprehensive spatial information from surrounding pixels. On the one hand, as shown from the first row of Fig. 1, the central pixel  $\mathbf{I}_c$  is rearranged each time with two pixels which are symmetrically located around it at all possible orientations, i.e. horizontal ( $0^\circ$ ), forward slant ( $45^\circ$ ), vertical ( $90^\circ$ ), and backward slant ( $135^\circ$ ), while from the second row, it can be seen that  $\mathbf{I}_c$  is sampled each time with four pixels. On the other side, it can be inferred from Fig. 2 that the  $3 \times 3$  square neighborhood is divided into four  $2 \times 2$  blocks where  $\mathbf{I}_c$  is sampled with three pixel in each direction.

It is appropriate to indicate that both mean grey value and median value are commonly used statistical metrics for texture modeling and analysis. In light of this and with the intention of generating a code that is impervious to noise and more resistant to lighting changes, various kinds of median and mean values are used as virtual pixels into the construction process of MTSP. Mathematical definitions of these values are given by the following equations (cf. Eqs. (8)–(13)):

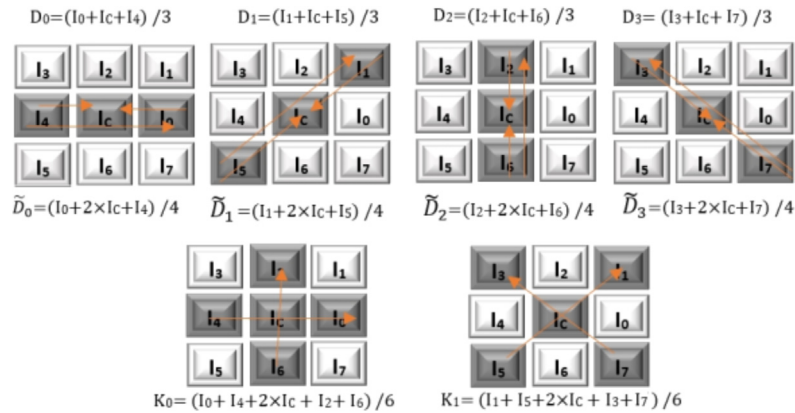


Fig. 1. Different template-directional neighborhood topologies.

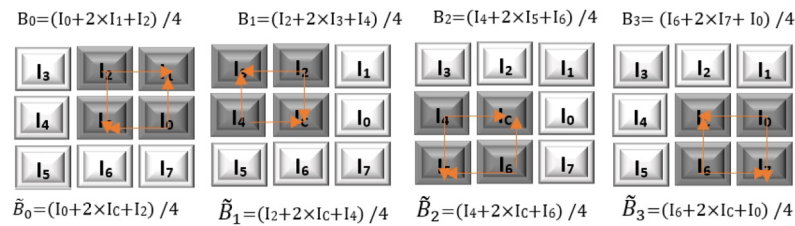


Fig. 2. Different template-block neighborhood topologies.

$$D_k = \frac{1}{3} (\mathbf{I}_k + \mathbf{I}_c + \mathbf{I}_{k+4}) \quad (8)$$

$$\tilde{D}_k = \frac{1}{4} (\mathbf{I}_k + 2\mathbf{I}_c + \mathbf{I}_{k+4}) \quad (9)$$

where  $\mathbf{D}_k$  and  $\tilde{\mathbf{D}}_k$  represent respectively the mean of  $(\mathbf{I}_k, \mathbf{I}_c, \mathbf{I}_{k+4})$  and the mean of  $((\mathbf{I}_k, \mathbf{I}_c), (\mathbf{I}_c, \mathbf{I}_{k+4}))$ , where  $k \in \{0, 1, 2, 3\}$ .

$$K_0 = \frac{1}{6} (\mathbf{I}_0 + \mathbf{I}_4 + 2\mathbf{I}_c + \mathbf{I}_2 + \mathbf{I}_6) \quad (10)$$

$$K_1 = \frac{1}{6} (\mathbf{I}_1 + \mathbf{I}_5 + 2\mathbf{I}_c + \mathbf{I}_3 + \mathbf{I}_7) \quad (11)$$

$$B_k = \frac{1}{4} (\mathbf{I}_{2k} + 2\mathbf{I}_{2k+1} + \mathbf{I}_{2k+2}) \quad (12)$$

$$\tilde{B}_k = \frac{1}{4} (\mathbf{I}_{2k} + 2\mathbf{I}_c + \mathbf{I}_{2k+2}) \quad (13)$$

where  $B_k$  and  $\tilde{B}_k$  represent respectively the mean of  $((\mathbf{I}_{2k}, \mathbf{I}_{2k+1}), (\mathbf{I}_{2k+1}, \mathbf{I}_{2k+2}))$  and the mean of  $((\mathbf{I}_{2k}, \mathbf{I}_c), (\mathbf{I}_c, \mathbf{I}_{2k+2}))$ , where  $k \in \{0, 1, 2, 3\}$ .

We consider  $(D_k, \tilde{D}_k)$  and  $(B_k, \tilde{B}_k)$  as virtual neighboring pixels of the central pixel  $\mathbf{I}_c$  and then compute their local means and medians as shown in the following equations (cf. Eqs. (14)–(19)):

$$m_D = \frac{1}{9} \left( \mathbf{I}_c + \sum_{k=0}^3 (D_k + \tilde{D}_k) \right) \quad (14)$$

$$m_B = \frac{1}{9} \left( \mathbf{I}_c + \sum_{k=0}^3 (B_k + \tilde{B}_k) \right) \quad (15)$$

$$m_I = \frac{\sum_{\alpha_1=1}^M \sum_{\alpha_2=1}^N \mathbf{I}(\alpha_1, \alpha_2)}{M \times N} \quad (16)$$

$$\hat{m}_D = \text{median}(D) \quad (17)$$

$$\hat{m}_B = \text{median}(B) \quad (18)$$

$$\hat{m}_I = \text{median}(I) \quad (19)$$

where  $B$  and  $D$  are the set of  $B_{k:k \in \{0,1,2,3\}}$  and  $D_{k:k \in \{0,1,2,3\}}$  (cf. Eqs. 8 and 12), respectively.

### 3.2. Coding scheme

First of all, in order to establish relationships between pixels and different sets of pixels, we use the set theory and in particular Venn diagrams which is a diagrammatic representation of different possible relationships between different sets of a finite number of elements. Let's consider the following definitions:

**Definition 1.** A set is an unordered collection of objects, called members or elements of the set. A real interval  $x$  is a nonempty set of real numbers  $A = [a, b] = \{x \mid a \leq x \leq b\}$  where  $a$  is called the infimum and  $b$  is called the supremum.

**Definition 2.** Let  $A$  and  $B$  be two sets. The set containing those elements in both  $A$  and  $B$  is the intersection of the sets  $A$  and  $B$ , indicated by  $A \cap B$ .

**Definition 3.** Let  $E$  be a set and  $A$  a subset of  $E$ . The complement of  $A$  in  $E$  is the set  $\{x \mid x \in E \text{ et } x \notin A\}$ . We denote it  $C_E A$  or  $E \setminus A$  or  $A^c$  or  $\bar{A}$ .

Accordingly, by considering the neighbouring pixels and the virtual pixels as well as their mean and median values, we construct six sampling sets denoted as  $\mathbb{S}_{i:i \in \{1, \dots, 6\}}$  (cf. Eqs. (20)–(25)).

$$\mathbb{S}_1 = \{D_0, D_1, \mathbf{I}_4, \mathbf{I}_5, \mathbf{I}_6, \mathbf{I}_7\} \quad (20)$$

$$\mathbb{S}_2 = \{D_2, D_3, \mathbf{I}_0, \mathbf{I}_1, \mathbf{I}_2, \mathbf{I}_3\} \quad (21)$$

$$\mathbb{S}_3 = \{m_I, K_0, \mathbf{I}_1, \mathbf{I}_3, \mathbf{I}_5, \mathbf{I}_7\} \quad (22)$$

$$\mathbb{S}_4 = \{\hat{m}_I, K_1, \tilde{B}_{k:k \in \{0, \dots, 3\}}\} \quad (23)$$

$$\mathbb{S}\mathbb{S}_5 = \left\{ \frac{\min(m_D, m_B)}{2}, \frac{\min(\hat{m}_D, \hat{m}_B)}{2}, \min(\tilde{D}_k, \tilde{B}_k)_{k \in \{0, \dots, 3\}} \right\} \quad (24)$$

$$\mathbb{S}\mathbb{S}_6 = \left\{ \frac{\max(m_D, m_B)}{2}, \frac{\max(\hat{m}_D, \hat{m}_B)}{2}, \dots, \max(\tilde{D}_k, \tilde{B}_k)_{k \in \{0, \dots, 3\}} \right\} \quad (25)$$

To visualize set operations, we define two kinds of Venn diagrams, i.e., Venn diagrams in lower and upper modes, as schematized in Figs. 3 and 4, respectively.

Given the defined six sampling sets  $\mathbb{S}\mathbb{S}_{i \in \{1, \dots, 6\}}$ , an ensemble of sets of pixels relationship based on three dynamic threshold values  $\tau_1, \tau_2$  and  $\tau_3$  are constructed according to both upper and lower Venn diagrams modes as well as the three definitions (given in Definition 1 to Definition 3). Denoted as  $\mathbb{A}$ , they are expressed as follows (cf. Eqs. (26)–(39)):

$$\mathbb{A}_1^U(\mathbf{x}) = \{\mathbf{x} \in \mathbb{S}\mathbb{S}_1 \mid \mathbf{x} \geq \mathbf{I}_c - \tau_1\} \quad (26)$$

$$\mathbb{A}_2^U(\mathbf{y}) = \{\mathbf{y} \in \mathbb{S}\mathbb{S}_2 \mid \mathbf{y} \geq \mathbf{I}_c + \tau_1\} \quad (27)$$

$$\mathbb{A}^U(\mathbf{x}, \mathbf{y}) = \mathbb{A}_1^U(\mathbf{x}) \cap \mathbb{A}_2^U(\mathbf{y}) \quad (28)$$

$$\mathbb{A}_1^L(\mathbf{x}) = \{\mathbf{x} \in \mathbb{S}\mathbb{S}_1 \mid \mathbf{x} \leq \mathbf{I}_c + \tau_1\} \quad (29)$$

$$\mathbb{A}_2^L(\mathbf{y}) = \{\mathbf{y} \in \mathbb{S}\mathbb{S}_2 \mid \mathbf{y} \leq \mathbf{I}_c - \tau_1\} \quad (30)$$

$$\mathbb{A}^L(\mathbf{x}, \mathbf{y}) = \mathbb{A}_1^L(\mathbf{x}) \cap \mathbb{A}_2^L(\mathbf{y}) \quad (31)$$

$$\mathbb{A}_3^U(\mathbf{x}) = \{\mathbf{x} \in \mathbb{S}\mathbb{S}_3 \mid \mathbf{x} \geq \mathbf{I}_c + \tau_2\} \quad (32)$$

$$\mathbb{A}_4^U(\mathbf{y}) = \{\mathbf{y} \in \mathbb{S}\mathbb{S}_4 \mid \mathbf{y} \geq \mathbf{I}_c - \tau_3\} \quad (33)$$

$$\mathbb{A}_5^U(\mathbf{z}) = \{\mathbf{z} \in \mathbb{S}\mathbb{S}_5 \mid \mathbf{z} \geq \mathbf{I}_c + \tau_1\} \quad (34)$$

$$\mathbb{A}^U(\mathbf{x}, \mathbf{y}, \mathbf{z}) = \mathbb{A}_3^U(\mathbf{x}) \cap \mathbb{A}_4^U(\mathbf{y}) \cap \mathbb{A}_5^U(\mathbf{z}) \quad (35)$$

$$\mathbb{A}_3^L(\mathbf{x}) = \{\mathbf{x} \in \mathbb{S}\mathbb{S}_3 \mid \mathbf{x} \leq \mathbf{I}_c - \tau_2\} \quad (36)$$

$$\mathbb{A}_4^L(\mathbf{y}) = \{\mathbf{y} \in \mathbb{S}\mathbb{S}_4 \mid \mathbf{y} \leq \mathbf{I}_c + \tau_3\} \quad (37)$$

$$\mathbb{A}_5^L(\mathbf{z}) = \{\mathbf{z} \in \mathbb{S}\mathbb{S}_6 \mid \mathbf{z} \leq \mathbf{I}_c - \tau_1\} \quad (38)$$

$$\mathbb{A}^L(\mathbf{x}, \mathbf{y}, \mathbf{z}) = \mathbb{A}_3^L(\mathbf{x}) \cap \mathbb{A}_4^L(\mathbf{y}) \cap \mathbb{A}_5^L(\mathbf{z}) \quad (39)$$

The local texture relationship between each points within the established six sampling sets  $\mathbb{S}\mathbb{S}_{i \in \{1, \dots, 6\}}$  and the central pixel, is encoded using three and seven-valued coding schemes (hence the name is ternary respectively septenary) according to the ensemble of sets of pixels relationship based on the three dynamic threshold values  $\tau_1, \tau_2$  and  $\tau_3$ . Note that  $\tau_1, \tau_2$  and  $\tau_3$  are employed to reduce the influence of outside factors like noise that disturbs patterns. We design a texture operator called Multi-scale Ternary and Septenary Pattern (MTSP) in order to clearly extract comprehensive micro structure features contained in these relationships. Conceptually, MTSP is composed of Single-scale Ternary Pattern (STP) and Single-scale Septenary Pattern (SSP) defined as follows:

### 3.2.1. Single-scale Ternary Pattern (STP)

By employing a three-valued coding scheme (i.e., concept of LTP-like methods), we design Single-scale Ternary Pattern (STP) to encode relationship between the central pixel and points of both the sampling sets  $\mathbb{S}\mathbb{S}_1$  and  $\mathbb{S}\mathbb{S}_2$ . The exploited indicator function  $\phi_{pattern}(\cdot)$  that converts each couple relationship in ternary form is given by Eq. 40.

$$\phi(\alpha) = \begin{cases} +1 & \text{if } \alpha \in \mathbb{A}^U(\mathbf{x}, \mathbf{y}) \\ 0 & \text{if } \alpha \in \mathbb{A}^U(\mathbf{x}, \mathbf{y}) \cap \mathbb{A}^L(\mathbf{x}, \mathbf{y}) \\ -1 & \text{if } \alpha \in \mathbb{A}^L(\mathbf{x}, \mathbf{y}) \end{cases} \quad (40)$$

The local information is then encoded using the following encoder noted STP and expressed as follows:

$$STP^{Pattern}(\mathbf{I}_c) = \sum_{p=0}^5 \phi_{pattern}(\mathbf{I}_p) \times 2^p \quad (41)$$

where

$$\phi_{pattern}(\mathbf{x}) = \{ 1 \text{ if } \phi(\mathbf{x}) = \{1, 2\} \text{ otherwise} \} \quad (42)$$

### 3.2.2. Single-scale Septenary Pattern (SSP)

Similarly to LQP which extended LTP method to five-value encoding technique and in order to capture more comprehensive features, in this paper, to encode relationship between points within the rest of sampling sets  $\mathbb{S}\mathbb{S}_{i \in \{3, \dots, 6\}}$  and the central pixel using a seven-value encoding scheme based on three dynamic threshold values ( $\tau_1, \tau_2$  and  $\tau_3$ ). Called Single-scale Septenary Pattern (SSP), it can capture discriminant micro structure information from the perspective of the established ensemble of

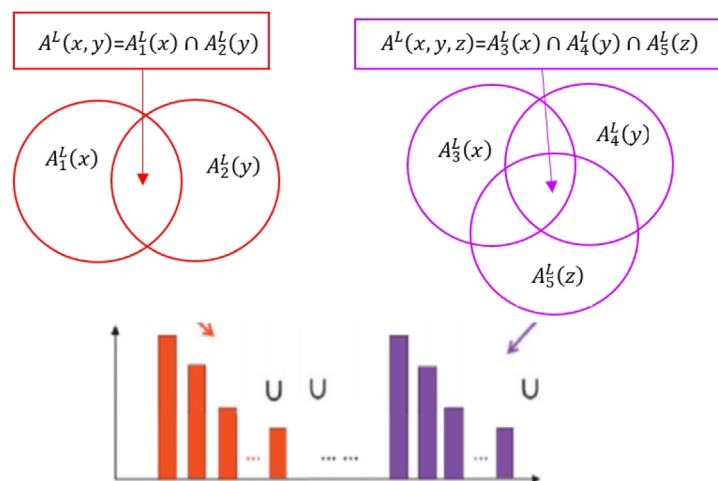


Fig. 3. A schematic image of the lower Venn diagrams mode.

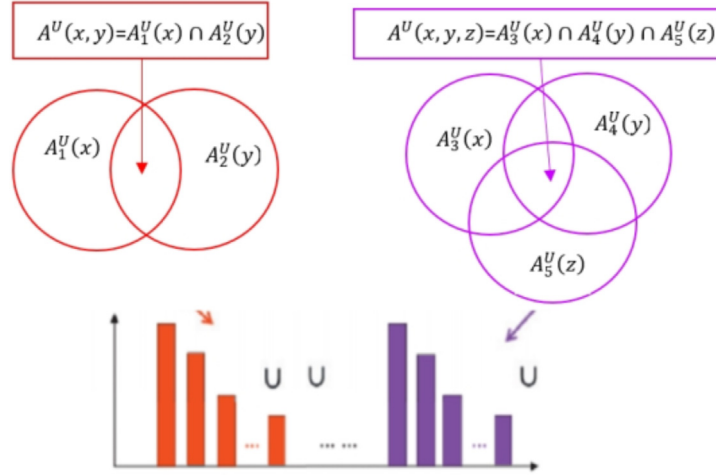


Fig. 4. A schematic image of the upper Venn diagrams mode.

sets of pixels relationship. SSP employs the following indicator denoted as  $\psi_{pattern}(\cdot)$  (cf. Eq. 45):

$$\psi(\alpha) = \begin{cases} +3 & \text{if } \alpha \in \mathbb{A}_3^U(\mathbf{x}) \cap \mathbb{A}_4^U(\mathbf{y}) \cap \overline{\mathbb{A}}^U(\mathbf{x}, \mathbf{y}, \mathbf{z}) \\ +2 & \text{if } \alpha \in \mathbb{A}_4^U(\mathbf{x}) \cap \mathbb{A}_5^U(\mathbf{y}) \cap \overline{\mathbb{A}}^U(\mathbf{x}, \mathbf{y}, \mathbf{z}) \\ +1 & \text{if } \alpha \in \mathbb{A}_3^U(\mathbf{x}) \cap \mathbb{A}_5^U(\mathbf{y}) \cap \overline{\mathbb{A}}^U(\mathbf{x}, \mathbf{y}, \mathbf{z}) \\ -1 & \text{if } \alpha \in \mathbb{A}_3^L(\mathbf{x}) \cap \mathbb{A}_5^L(\mathbf{y}) \cap \overline{\mathbb{A}}^L(\mathbf{x}, \mathbf{y}, \mathbf{z}) \\ -2 & \text{if } \alpha \in \mathbb{A}_4^L(\mathbf{x}) \cap \mathbb{A}_5^L(\mathbf{y}) \cap \overline{\mathbb{A}}^L(\mathbf{x}, \mathbf{y}, \mathbf{z}) \\ -3 & \text{if } \alpha \in \mathbb{A}_3^L(\mathbf{x}) \cap \mathbb{A}_4^L(\mathbf{y}) \cap \overline{\mathbb{A}}^L(\mathbf{x}, \mathbf{y}, \mathbf{z}) \\ 0 & \text{otherwise} \end{cases} \quad (43)$$

where  $\overline{\mathbb{A}}^U(\mathbf{x}, \mathbf{y}, \mathbf{z})$  (resp.  $\overline{\mathbb{A}}^L(\mathbf{x}, \mathbf{y}, \mathbf{z})$ ) is the complement of  $\mathbb{A}^U(\mathbf{x}, \mathbf{y}, \mathbf{z})$  (resp.  $\mathbb{A}^L(\mathbf{x}, \mathbf{y}, \mathbf{z})$ ) as defined in Definition 2.

The local information is then encoded using the following encoder noted SSP and expressed as follows:

$$SSP^{Pattern}(\mathbf{I}_c) = \sum_{p=0}^5 \psi_{pattern}(\mathbf{I}_p) \times 2^p \quad (44)$$

where  $pattern \in \{1, 2, 3, 4, 5, 6\}$  are six binary patterns by taking into account its lower-positive, lower-negative, upper-positive, upper-negative, middle-positive and middle-negative components denoted as  $\psi(+3), \psi(+2), \psi(+1), \psi(-1), \psi(-2)$  and  $\psi(-3)$  respectively. It is worth noting that SSP encodes a texture image in seven channels but gives six bit patterns. The resultant image encoded by SSP is divided into six bit patterns using the  $\psi_{pattern}$  function defined by (cf. Eq. 45):

$$\psi_{pattern}(\mathbf{x}) = \{1 \text{ if } \psi(\mathbf{x}) = \{1, 2, 3, 4, 5, 6\} \text{ otherwise} \} \quad (45)$$

### 3.3. Features extraction

At this step, two code maps are generated for each grayscale image using both the STP and SSP encoders. Two histograms are then produced from these two code maps using Eqs. 46 and 47.

$$\mathbf{h}_{STP}(\mathbf{k}) = \sum_{\mathbf{I}_c \in \mathbf{I}} \widehat{\delta}(STP(\mathbf{I}_c), \mathbf{k}) \quad (46)$$

$$\mathbf{h}_{SSP}(\mathbf{k}) = \sum_{\mathbf{I}_c \in \mathbf{I}} \widehat{\delta}(SSP(\mathbf{I}_c), \mathbf{k}) \quad (47)$$

where  $\mathbf{k} \in [0, 2^6]$  is the number of STP and SSP patterns and  $\widehat{\delta}(\cdot)$  is the Kronecker delta function given by (cf. Eq. 48):

$$\widehat{\delta}(\alpha, \beta) = \begin{cases} 1 & \text{if } \alpha = \beta \\ 0 & \text{otherwise} \end{cases} \quad (48)$$

Considering the fact that several texture features have different capabilities to describe images and in order to take advantage of their performances, the trend towards integrating them into a single row feature vector seems to be the best way forward. To accomplish such a task and to capture more salient texture features, a multi-scale fusion operation is used to generate a novel hybrid texture description model. The obtained texture operator, which is the fusion of both STP and SSP operators is called multi-scale ternary and septenary pattern (MTSP). It is expected to be more powerful as it leads to improved power of discrimination and expressiveness of STP and SSP operators via their complementary informations. The generated single feature vector of multi-scale analysis is expressed as follows:

$$\mathbf{h}_{MTSP} = \langle \mathbf{h}_{STP}, \mathbf{h}_{SSP} \rangle \quad (49)$$

where  $\langle \cdot \rangle$  is the concatenation operator.

### 3.4. Dynamic thresholds

In order to realize a high trade-off between classification accuracy and computational efficiency, we plan to define locally and dynamically the three parameters  $\tau_1, \tau_2$  and  $\tau_3$  of MTSP. Given a  $3 \times 3$  square neighborhood, we first calculate the neighbor to center difference to form a difference vector  $dv_{3 \times 3}$  (cf. Eq. 50). After that, the mean of all negative and positive difference values (i.e.,  $dv_{3 \times 3}^{mean-}$  and  $dv_{3 \times 3}^{mean+}$ , respectively) are produced (cf. Eqs. 51 and 52).

$$dv_{3 \times 3} = \left[ \frac{1}{2}(\mathbf{I}_0 - 3 * \mathbf{I}_c), \frac{1}{2}(\mathbf{I}_1 - 3 * \mathbf{I}_c), \dots, \frac{1}{2}(\mathbf{I}_7 - 3 * \mathbf{I}_c) \right] \quad (50)$$

$$dv_{3 \times 3}^{mean+} = \frac{1}{pv} \sum_{k=1}^{pv} dv_k^+ \quad (51)$$

$$dv_{3 \times 3}^{mean-} = \frac{1}{nv} \sum_{k=1}^{nv} |dv_k^-| \quad (52)$$

where  $dv_k^+$  and  $dv_k^-$  are, respectively, the negative (i.e.,  $\frac{1}{2}(\mathbf{I}_k - 3 * \mathbf{I}_c) < 0$ ) and positive (i.e.,  $\frac{1}{2}(\mathbf{I}_k - 3 * \mathbf{I}_c) \geq 0$ ) difference values in the  $dv_{3 \times 3}$  set,  $nv$  is the number of  $dv_k^-$  elements and  $pv$  is the number of  $dv_k^+$  elements ( $pv + nv = P$ ). Finally, the parameters

$\tau_1, \tau_2$  and  $\tau_3$  are calculated using these equations (cf. Eqs. (53)–(55)):

$$\tau_1 = \frac{|dv_{3 \times 3}^{\text{mean}^+} - dv_{3 \times 3}^{\text{mean}^-}|}{\max(dv_{3 \times 3}^{\text{mean}^+}, dv_{3 \times 3}^{\text{mean}^-})} \quad (53)$$

$$\tau_2 = \frac{dv_{3 \times 3}^{\text{mean}^+} + dv_{3 \times 3}^{\text{mean}^-}}{\min(dv_{3 \times 3}^{\text{mean}^+}, dv_{3 \times 3}^{\text{mean}^-})} \quad (54)$$

$$\tau_3 = \frac{1}{2}(\tau_1 + \tau_2) \quad (55)$$

**Algorithm 1** illustrates the pseudo-code of the designed MTSP descriptor.

#### Algorithm 1. Computing MTSP method

---

**Require:**  $I \leftarrow$  grayscale texture image  $I_{M \times N}$ .  
**Output:**  $\mathbf{h}_{\text{MTSP}} \leftarrow$  the multi-scale histogram feature.

- 1: Obtain the median of the grey-scale values  $\tilde{m}_1$  of the whole image  $I_{M \times N}$  using Eq. 19.
- 2: Obtain the average global gray levels  $m_1$  of the whole image  $I_{M \times N}$  using Eq. 16
- 3: **for** Each central pixel  $\mathbf{I}_c$  of  $I_{M \times N}$  **do**
- 4: Consider a grayscale image patch of dimension  $3 \times 3$  around  $\mathbf{I}_c$ .
- 5: Obtain the difference between the central pixel and its surrounding pixels  $df_{3 \times 3}$  and then obtain the dynamic thresholds  $\tau_1, \tau_2$  and  $\tau_3$  using Eqs. (53)–(55), respectively.
- 6: Obtain local means of the virtual pixels  $(D_k, \tilde{D}_k)$  and  $(B_k, \tilde{B}_k)$  using Eqs. 14 and 15.
- 7: Obtain local medians of the virtual pixels  $(D_k, \tilde{D}_k)$  and  $(B_k, \tilde{B}_k)$  using Eqs. 17 and 18.
- 8: Obtain (using Eqs. 41 and 44, respectively):
  - $STP^{\text{Pattern}}(\mathbf{I}_c) \leftarrow$  the single-scale ternary pattern (STP) based on indicator function  $\phi_{\text{pattern}}(\cdot)$  and associated to the set of pixels relationship  $\mathbb{A}^U(\mathbf{x}, \mathbf{y})$  and  $\mathbb{A}^L(\mathbf{x}, \mathbf{y})$ .
  - $SSP^{\text{Pattern}}(\mathbf{I}_c) \leftarrow$  the single-scale septenary pattern (SSP) based on indicator function  $\psi_{\text{pattern}}(\cdot)$  and associated to the set of pixels relationship  $\mathbb{A}_3^U(\mathbf{x}), \mathbb{A}_4^U(\mathbf{x}), \mathbb{A}_5^U(\mathbf{x}), \mathbb{A}_5^L(\mathbf{x}), \mathbb{A}_4^L(\mathbf{x}), \mathbb{A}_3^L(\mathbf{x}), \overline{\mathbb{A}}^U(\mathbf{x}, \mathbf{y}, \mathbf{z})$  and  $\overline{\mathbb{A}}^L(\mathbf{x}, \mathbf{y}, \mathbf{z})$ .
- 9: **end for**
- 10: Obtain (using Eqs. 46 and 47, respectively):
  - $\mathbf{h}_{\text{STP}}(\mathbf{k}) \leftarrow$  histogram feature of  $STP^{\text{Pattern}}(\mathbf{I}_c)$  code map.
  - $\mathbf{h}_{\text{SSP}}(\mathbf{k}) \leftarrow$  histogram feature of  $SSP^{\text{Pattern}}(\mathbf{I}_c)$  code map.
- 11: Obtain the multi-scale histogram feature  $\mathbf{h}_{\text{MTSP}}$  using Eq. 49.
- 12: **return**  $\mathbf{h}_{\text{MTSP}}$

---

## 4. Experimental results and discussion

In this section, the efficiency and performance of the proposed MTSP descriptor were extensively evaluated on several publicly available texture datasets and compared to 19 recent state-of-the-art methods using a series of experiments (cf. Table 2). The experiments herein were conducted under the split-sample validation protocol where half of the samples are randomly chosen for training and the rest of samples are used for testing. The 1-NN technique with L1-city block distance is used for classification purpose. Let us stress out that the classification experiments are repeated over 100 random splits to avoid any bias resulting from the database's partition, and estimated accuracies is measured as

averaged results. In the following, the considered texture databases and the impact of feature combination process of the two SSP and STP encoders are first presented and the findings of the experiments are then discussed.

### 4.1. Texture datasets

To further verify the capabilities and performance stability of MTSP, extensive experiments are carried out on ten well-known datasets such as JerryWu, KTH-TIPS2b, BonnBTF, MBT, Kylberg, Brodatz, VisTex, CURETgrey and KTH-TIPS (the same datasets used in (Rachdi et al., 2020)) and STex. These considered datasets were selected to cover different representative characteristics in terms of number of images and classes, and specific challenges. It can be inferred from Table 1 that each database presents specific challenges in terms of translation, scale, view angle, rotation, illumination, etc., allowing thus to evaluate the performance of the tested existing methods as well as the designed descriptor against these factors.

### 4.2. Impact of feature combination process

As pointed out previously, the combination of different feature extraction methods is suitable to exploit their advantages simultaneously with the objective of strengthening the discriminant power of the produced encoder and promote the overall classification results. MTSP is composed of two encoders namely STP and SSP and in order to highlight the impact of the combination process, we evaluate the MTSP performance compared to its STP and SSP components applied alone. Fig. 5 illustrates the comparison results obtained using KTH-TIPS2b, VisTex, MBP, CURET and STex datasets. It can be inferred from Fig. 5 that none of the two encoders gives always the best score against the other, i.e., there are some datasets where STP achieves the best accuracies against SSP and vice versa. Remarkably, we can notice that MTSP, as a hybrid texture description model which extracts complementary texture information from combined components, improves significantly the classification results of both STP and SSP encoders applied alone giving reasons thus for their combination.

### 4.3. Comparative assessment of performance

#### 4.3.1. Experiment #1: Investigation on performance stability

Table 2 summarizes the achieved average classification accuracies (i.e., over 100 splits) of each tested method over each dataset as well as the GAP (global average performance) over all the ten used datasets.

Concerning the results shown in Table 2, one can notice that some handcrafted descriptors LDENP, DC and EULLTP are emerged in majority of cases as the three weakest methods of the panel (illustrated in bolditalic) and on almost all the used database.

The majority of the tested methods with the obvious exception of those previously mentioned, produces promising classification results on KTH-TIPS database (dataset 4 in Table 2) with a score exceeds 97%. Moreover, some methods like DNT-MQP, LETRIST, MNTCDP, LDEBP, etc. and the proposed MTSP to get the score of 100%, leaving then potentially no possibility for improvement. This same observation can be made for Brodatz dataset (database 3 in Table 2) where MTSP as well as various evaluated existing methods are able to accurately discern between all classes.

The performance of all the tested methods degrades considerably on VisTex and MBT datasets (datasets 6 and 7 in Table 2) where the achieved scores do not exceed respectively 81% and 88% (obtained with the proposed method). The overall performance may be improved if more complicated machine learning

**Table 1**

Image databases considered in this work. The Table illustrates the properties of each database, including the variety of samples in view point, rotation, illumination changes, scale, the number of classes, etc.

No.	Name	Classes	Total samples	Challenges
1	Jerry Wu	39	156	Images captured under different imaging direction, surface rotation and illumination direction.
2	Bonn BTF	10	160	Images captured under varying illumination and viewing angle.
3	Brodatz	13	208	Images are not-corrected and acquired with a lack of intraclass variations and without controlled conditions.
4	KTH-TIPS	10	40	Images captured under three poses, nine illumination conditions and nine scales.
5	KTH-TIPS2b	11	176	Image captured under pose scale, rotation and illumination changes.
6	VisTex	167	2672	Images captured under real world conditions.
7	MBT	154	2464	Images in high spatial resolution, which are common in areas such as remote sensing and astronomy.
8	Kylberg	28	4480	Images are corrected for aberration, vignetting and lens distortion and captured under controlled conditions.
9	CURET	61	5612	Images with photometric and geometric properties as variations in illumination, viewing angle and rotation.
10	STex	476	7616	Images representing scenes, materials and objects, such as leather, buildings, bark, metal, flowers, etc.

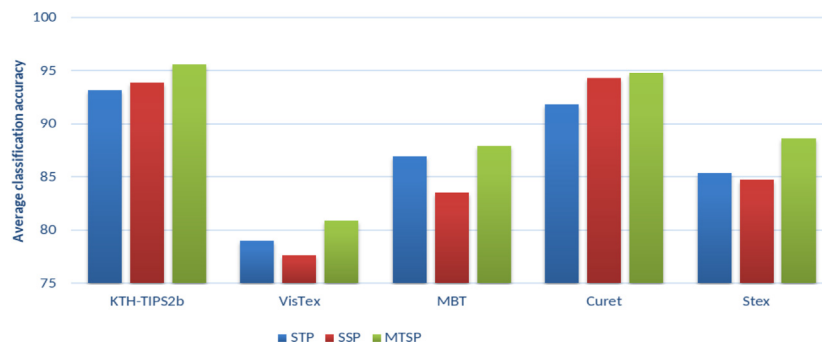


**Fig. 5.** Accuracies obtained with single-scale image descriptors as well as their combinations.

**Table 2**

Overall accuracy by method and texture dataset. The last column represents the GAP of each descriptor over all the considered databases. The best method over each dataset is highlighted in bold, the three worst in bolditalic. As a bold and bolditalic texture operator, QxLBP is assessed only on bold and bolditalic texture databases (it is tested with pyramid level L=3 as it gives the highest scores).

Descriptor	Reference	Year	1	2	3	4	5	6	7	8	9	10	GAP	Rank
<b>MTSP</b>	this paper	-	<b>100</b>	<b>100</b>	<b>100</b>	<b>100</b>	<b>95.61</b>	<b>80.93</b>	<b>87.96</b>	99.71	94.98	<b>88.66</b>	<b>94.766</b>	1
STP	this paper	-	99.54	99.97	99.99	100.00	93.16	78.97	86.93	98.62	91.86	85.38	93,442	2
SSP	this paper	-	99.83	99.96	99.95	100.00	93.86	77.68	83.57	99.80	94.32	84.73	93,37	3
LBP	(Ojala et al., 1996)	1996	97,26	95,86	100	100	89,67	74,19	85,61	97,07	90,71	79,73	91,01	4
LTP	(Tan and Triggs, 2010)	2010	98,06	98,64	100	100	92,92	75,38	88,56	98,96	90,26	81,38	92,416	5
DNT-MQP	(Rachdi et al., 2020)	2021	99,88	99,25	100	100	95,12	78,22	86,91	99,86	95,32	87,8	94,238	6
FLNIP	(Ghose et al., 2020)	2020	97,91	95,42	100	100	93,78	78,42	86,92	99,14	93,45	85,51	93,055	7
RALBGC	(El Khadiri et al., 2018)	2018	97,51	98,8	100	100	93,39	77,89	86,22	99,09	93,31	83,77	92,998	8
ARCSLBP	(Ruichek, 2019)	2018	99,53	99,17	99,88	100	93,23	75,76	83,23	99,8	94,03	83,25	92,788	9
MNTCDP	(Kas et al., 2018)	2018	100	100	100	100	90,93	79,53	78,95	98,48	92,4	86,27	92,656	10
ILQP	(Armi and Fekri-Ershad, 2019)	2019	98,03	98,72	100	100	93,39	75,39	85,8	98,33	91,03	83,21	92,39	11
LETRIST	(Song et al., 2017)	2018	100	100	99,95	100	94	70,16	80,12	<b>99,88</b>	97,08	81,41	92,258	12
KLBP	(Tuncer and Dogan, 2020)	2019	97,49	97,34	100	100	91,24	76,36	86,78	98,6	91,12	82,49	92,142	13
LQP	(Nanni et al., 2010)	2010	97,72	97,34	100	100	90,55	76,58	86,76	98,28	91,21	82,35	92,079	14
LDTP	(El-khadiri et al., 2018)	2018	98,23	99,88	100	100	90,47	76,76	82,97	97,74	91,54	82,97	92,056	15
LOOP	(Chakraborti et al., 2018)	2018	96,86	98,78	99,97	100	85,81	73,25	83,99	97,75	90,61	77,81	90,483	16
LDEBP	(Sucharitha and Senapati, 2019)	2019	98,87	<b>92,96</b>	99,96	100	87,3	71,26	84,15	98,8	89,33	82,11	90,474	17
LDZP	(Roy et al., 2018)	2019	96,72	96,85	100	99,75	88,53	68,62	84,18	<b>92,5</b>	84,84	71,07	88,306	18
LGONBP	(Song et al., 2020)	2021	99,35	99,28	99,84	100	85,51	<b>54,62</b>	72,31	99,85	<b>97,21</b>	69,51	87,748	19
LNIP	(Banerjee et al., 2018)	2019	96,86	<b>77,86</b>	99,73	<b>98,45</b>	82,97	72,42	83,99	96,55	85,88	78,29	87,3	20
<b>DC</b>	(Ouslimani et al., 2019)	2018	<b>94,95</b>	93,36	<b>99,48</b>	100	<b>79,78</b>	58,6	<b>56,24</b>	97,92	<b>80,67</b>	<b>51,94</b>	<b>81,294</b>	21
<b>EULLTP</b>	(Kabbai et al., 2019)	2019	<b>92,58</b>	93,4	<b>99,38</b>	<b>93,9</b>	<b>78,63</b>	<b>53,53</b>	<b>71,75</b>	<b>94,87</b>	<b>73,35</b>	<b>58,26</b>	<b>80,965</b>	22
<b>LDENP</b>	(Pillai et al., 2018)	2018	<b>88,5</b>	<b>88,29</b>	<b>95,4</b>	<b>88,8</b>	<b>65,8</b>	<b>48,93</b>	<b>60,4</b>	<b>87,13</b>	<b>64,61</b>	<b>43,43</b>	<b>73,129</b>	23
QxLBP	(Song et al., 2021)	2021	-	-	-	-	-	-	70,05	-	-	74,03	72,04	24

algorithms such as extended nearest neighbor (ENN) and SVM are used instead of the 1-NN classifier.

Moreover, none of the existing methods achieve good performance on all the used datasets. Indeed, it is important to note that obtaining good results on certain datasets, does not necessarily ensure obtaining satisfactory classification results on the others. LGONBP illustrates clearly this behavior where it can be seen that it realizes outstanding scores on six databases out of ten, but no on KTH-TIPS2b (dataset 5), VisTex (dataset 6), MBT (dataset 7) and

STex (dataset 10 in Table 2) datasets. Indeed, the realized scores decline dramatically compared to the MTSP operator (i.e., the top 1 descriptor). This same observation is valid for several other texture operators such as LETRIST, LQP, EULLTP and DC and so on.

It can also be inferred from Table 2 that MTSP offers satisfactory classification results and positions itself as the best texture operator as it works meaningfully better for eight datasets out of ten: Jerry Wu, Bonn BTF, Brodatz, KTH-TIPS, KTH-TIPS2b, Vistex, MBT and STex (databases 1 to 7 and 10 in Table 2) with a score upper

than 80.93 %. It obtains the best rank with a score equal to 94.76 % when we consider the global average performance (GAP) against all the existing descriptors. Furthermore, it is in the top 5 and 4 texture operators on Kylberg and CUREt datasets, respectively. Nevertheless, let us mention that when MTSP does not realize the highest overall accuracies, it yields an interesting competitive score compared to the one realized by the top 1 method. Taking the Kylberg database as an example (database 8 in Table 2), MTSP is ranked at the 5th best position (i.e., MTSP has the fifth-highest accuracy), but in contrast, it reached a score of 99.71% which is seen as a very satisfying result as it is very close to the one of the texture operator ranked at the first position reaching a score of 99.88%. Remarkably, MTSP provides superior scores against QxLBP, which was originally conceived for color image representation, on MBT and STex color texture databases. QxLBPP, like a large number of color image descriptors, shows a tendency to be more sensitive to resolution and illumination. Additionally, it typically either ignores spatial correlations between pixels in the image or gives them less weight (Rachdi et al., 2020).

It is interesting to note that the satisfactory results realized on KTH-TIPS2b and Jerry Wu indicate that MTSP can tolerate a certain degree of rotation variations. Good performance on these two datasets indicate that MTSP shows reasonable tolerance to rotation when compared to LETRIST, which was originally designed for rotation-invariant texture description. In particular, MTSP gives 95.61% on KTH-TIPS2b vs 90.08% by LETRIST, indicating a performance improvement about 5,53%. Furthermore, the good scores of MTSP (upper 94,98%) on Jerry Wu, Bonn BTF, KTH-TIPS2b, KTH-TIPS, CUREt, and Kylberg datasets indicate that MTSP has good tolerance to illumination changes. The significant accuracy (100%) obtained on KTH-TIPS2b indicate that MTSP has also good tolerance to scale changes.

Considering the findings above, it can be concluded that the developed handcrafted MTSP method, despite its smaller feature vector length ( $2^8$  codes), is relatively efficient. The proposed method ranks first with scores that are relatively high and stable against the 19 evaluated existing methods on almost all the 10 several texture databases used. These findings indicate that the combination of both STP and SSP features describes better the characteristics of texture images helping thus to construct a descriptor that works well on various texture databases.

#### 4.3.2. Experiment #2: Statistical significance of the achieved results in terms of accuracy improvement

The purpose of this section is to further prove statistically the realized performances via MTSP vs the existing evaluated methods by employing the ranking procedure based on the Wilcoxon signed rank test introduced in Ruichek (2018). The algorithm is applied on all the pairwise combinations of the 19 evaluated existing texture operators including MTSP on the ten tested databases. Table 3 shows the reached ranking results according to the normalized number of victories (number of wins/(number of used databases\* (number of evaluated methods - 1))) realized by each descriptor on all the considered databases. Fig. 6 illustrates the produced classification results in the form of a scatter plot. The Xaxis is the dimension of feature vectors (on log 2 scale), while the Y axis is the normalized number of victories reached by each evaluated texture operator.

It emerges from both Table 3 and Fig. 6 that the conclusions that can be highlighted from the analysis of the realized results are coherent with those drawn previously in Section 4.3.1. Indeed, these results reinforce the conclusion that the combination of both STP and SSP is capable of representing local texture well which allows to construct a texture descriptor which is clearly the most effective descriptor among all the others methods. In particular,

**Table 3**

Ranking results obtained using the Wilcoxon-based ranking test according to the normalized number of victories reached by each evaluated texture operator on all the employed databases.

Ranking	1-NN	Texture descriptor	Victories/comparisons	Dimension
1		MTSP	0.788	256
2		DNT-MQP	0.738	384
3		FLNIP	0.600	1024
4		MNTCDP	0.588	2048
5		LETRIST	0.572	413
6		ARCSLBP	0.566	256
7		RALBGC	0.561	1022
8		ILQP	0.483	1024
9		LDTF	0.477	1022
10		KLBP	0.466	1280
11		LQP	0.461	1024
12		LGONBP	0.427	1404
13		LDEBP	0.366	64
14		LOOP	0.311	256
15		LDZP	0.261	354
16		LNIP	0.216	512
17		DC	0.122	225
18		EULLTP	0.077	32
19		LDENP	0.011	15

the normalized number of victories realized by MTSP is 0.788, vs. 0.738 with DNT-MQP (top 2<sup>nd</sup>). vs. 0.60 with FLNIP vs. 0.588 with MNTCDP vs. 0.572 with LETRIST, etc. As mentioned previously, MTSP is based on the LQP concept. Hence, if we consider the performance of LQP as the benchmark, MTSP gives about 71,73% improvement over the ten used databases.

## 5. Implementation and reproducible research

The experiments herein was carried out on a laptop equipped with 2.10 GHz Core i7 CPU, 8 GB of RAM and having Ubuntu 14.04 trusty operating system. The evaluated methods have been implemented in MATLAB R2013a. Fig. 7 illustrates the processing time (in minutes) over 2464 samples of the MBT dataset (dataset 7 in Table 1), including computation of feature extraction, distance calculation and 1-NN classification, for all the evaluated methods. It is clear that the designed MTSP texture operator makes the best compromise between computational cost and classification performance.

## 6. Conclusion

In this paper, we have proposed an efficient feature descriptor referred to as Multi-scale Ternary and Septenary Pattern (MTSP) based on multiple oriented blocks and directions based neighborhood topologies as well the set theory. MTSP combines the concepts of both LQP and LTP-like descriptors in the same compact encoding scheme to encode the interactions between pixels within  $3 \times 3$  grayscale image patch. The capabilities and performance stability of MTSP have been evaluated on ten challenging texture databases using 1-NN classifier against 19 recent and advanced state-of-the-art texture operators. MTSP descriptor showed considerable performance over all used databases, indicating that it better describes the characteristics of texture images.

## 7. Limitations and future work

The proposed texture operator requires images to be converted to grayscale before any transformation step. Thus, one of the limitations of the proposed method is that it is mathematically and theoretically unsuitable for direct application to color images. As

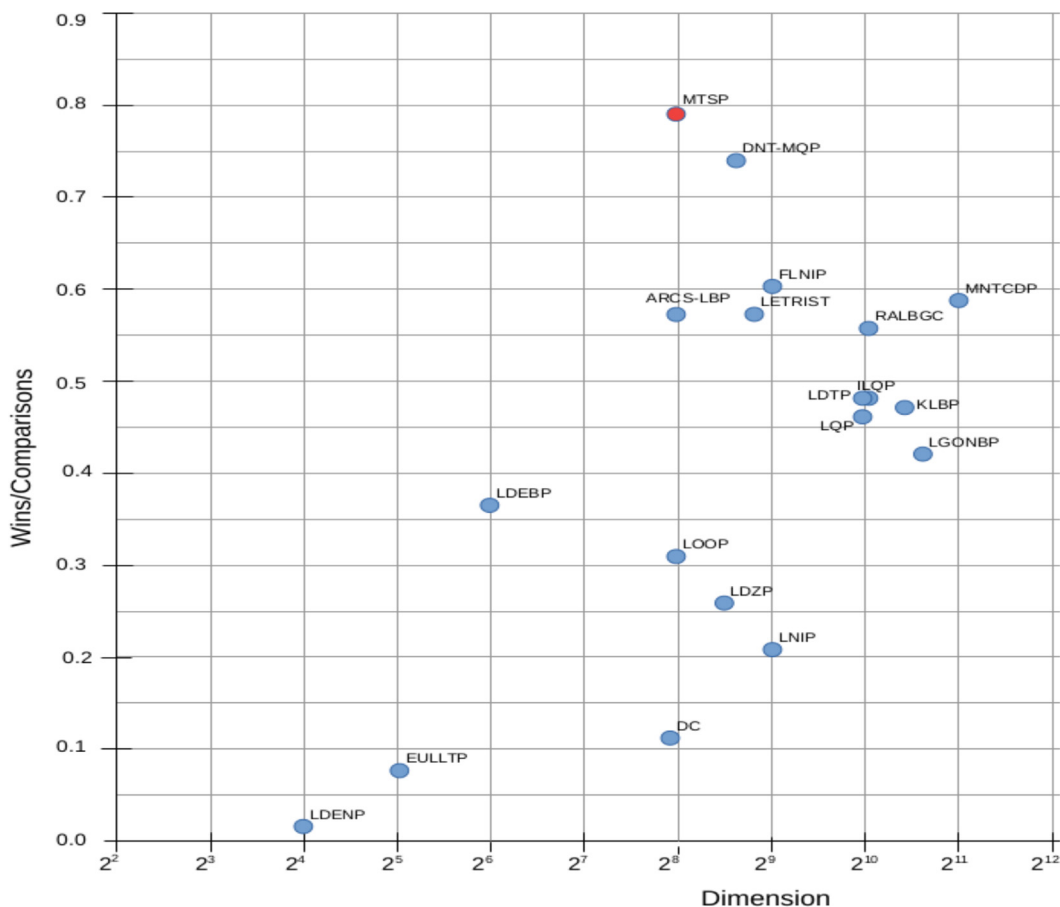


Fig. 6. Ranking results on all the used databases. Blue and orange dots indicate, respectively, the evaluated state-of-the art methods and the proposed method.

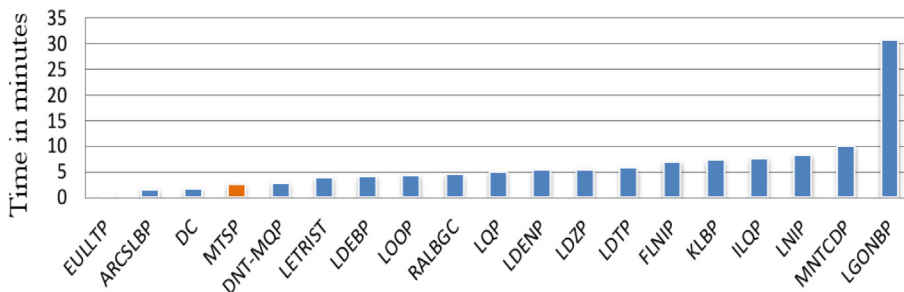


Fig. 7. The processing time (in minutes) of the evaluated methods.

indicated in the analysis of the results, all the evaluated methods as well as the proposed descriptor show their weaknesses in classifying images captured under real world conditions and or those presenting high spatial resolution, which indicates that the proposed method is less tolerant to ambiguities due to complex image patterns and different kinds of disturbances. Furthermore, the construction process of the proposed method only considers a unit distance radius and the sampling neighbourhood P and sampling radius R parameters have not been fully investigated.

In future work, we plan to test other sophisticated classifiers in the aim of increasing the classification rate. We plan also to extend the proposed descriptor in order to exploit color information and therefore explore its applicability for the classification of color textures. We suggest directing our research work towards the incorporation of the proposed descriptor into deep architectures.

### Declaration of Competing Interest

The authors declare that they have no known competing financial interests or personal relationships that could have appeared to influence the work reported in this paper.

### References

Al Saida, I., Rziza, M., Debayle, J., 2022. A New LBP Variant: Corner Rhombus Shape LBP (CRSLBP). *J. Imag.* 8 (7), 200.  
 Armi, L., Fekri-Ershad, S., 2019. Texture image Classification based on improved local Quinary patterns. *Multimedia Tools Appl.* 78 (14), 18995–19018.  
 Bahram, T., 2022. A texture-based approach for offline writer identification. *J. King Saud Univ.-Comput. Informat. Sci.*  
 Banerjee, P., Bhunia, A.K., Bhattacharyya, A., Roy, P.P., Murala, S., 2018. Local neighborhood intensity pattern—a new texture feature descriptor for image retrieval. *Expert Syst. Appl.* 113, 100–115.

- Banerjee, P., Bhunia, A.K., Bhattacharyya, A., Roy, P.P., Murala, S., 2018. Local Neighborhood Intensity Pattern-A new texture feature descriptor for image retrieval. *Expert Syst. Appl.* 113, 100–115.
- Bhattacharjee, D., Roy, H., 2021. Pattern of local gravitational force (PLGF): A novel local image descriptor. *IEEE Trans. Pattern Anal. Machine Intell.* 43 (2), 595–607.
- Chakraborti, T., McCane, B., Mills, S., Pal, U., 2018. LOOP Descriptor: Local Optimal-Oriented Pattern. *IEEE Signal Process. Lett.* 25 (5), 635–639.
- Chakraborty, S., Singh, S.K., Chakraborty, P., 2017. Local quadruple pattern: A novel descriptor for facial image recognition and retrieval. *Comput. Electr. Eng.* 62, 92–104.
- Chakraborty, S., Singh, S.K., Chakraborty, P., 2018. Centre symmetric quadruple pattern: A novel descriptor for facial image recognition and retrieval. *Pattern Recogn. Lett.* 115, 50–58.
- Cohen, F.S., Fan, Z., Patel, M.A., 1991. Classification of rotated and scaled textured images using Gaussian Markov random field models. *IEEE Trans. Pattern Anal. Mach. Intell.* 13 (02), 192–202.
- Davis, L.S., 1981. Polarograms: a new tool for image texture analysis. *Pattern Recogn.* 13 (3), 219–223.
- Dawood, H., Saleem, S., Hassan, F., Javed, A., 2022. A robust voice spoofing detection system using novel CLS-LBP features and LSTM. *J. King Saud Univ.-Comput. Informat. Sci.*
- El Idrissi, A., El merabet, Y., Ruichek, Y., 2020. Palmprint recognition using state-of-the-art local texture descriptors: a comparative study. *IET Biomet.* 9 (4), 143–153.
- El-khadiri, I., Chahi, A., El-merabet, Y., Ruichek, Y., Touahni, R., 2018. Local directional ternary pattern: A new texture descriptor for texture classification. *Comput. Vis. Image Underst.* 169, 14–27.
- El Khadiri, I., Kas, M., El Merabet, Y., Ruichek, Y., Touahni, R., 2018. Repulsive-and-attractive local binary gradient contours: New and efficient feature descriptors for texture classification. *Inf. Sci.* 467, 634–653.
- El khadiri, I., El merabet, Y., Ruichek, Y., Chetverikov, D., Touahni, R., 2020. O3S-MTP: Oriented star sampling structure based multi-scale ternary pattern for texture classification. *Signal Process.: Image Commun.* (2020), 115830.
- El Khadiri, I., El merabet, Y., Tarawneh, A.S., Ruichek, Y., Chetverikov, D., Touahni, R., Hassanat, A.B., 2021. Petersen Graph Multi-Orientation Based Multi-Scale Ternary Pattern (PGMO-MSTP): An Efficient Descriptor for Texture and Material Recognition. *IEEE Trans. Image Process.* 30, 4571–4586.
- Fernandez, A., Alvarez, M.X., Bianconi, F., 2011. Image classification with binary gradient contours. *Opt. Lasers Eng.* 49 (9–10), 1177–1184.
- Fernandez, A., Alvarez, M.X., Bianconi, F., 2011. Image classification with binary gradient contours. *Opt. Lasers Eng.* 49 (9–10), 1177–1184.
- Ghose, S., Das, A., Bhunia, A.K., et al., 2020. Fractional Local Neighborhood Intensity Pattern for Image Retrieval using Genetic Algorithm. *Multimed Tools Appl.* 79, 18527–18552.
- Guo, Z., Zhang, L., Zhang, D., 2010. A completed modeling of local binary pattern operator for texture classification. *IEEE Trans. Image Process.* 19 (6), 1657–1663.
- Guo, Z., Li, Q., You, J., Zhang, D., Liu, W., 2012. Local directional derivative pattern for rotation invariant texture classification. *Neural Comput. Appl.* 21 (8), 1893–1904.
- Hadid, A., Ylioinas, J., Bengherabi, M., Ghahramani, M., Taleb-Ahmed, A., 2015. Gender and texture classification: A comparative analysis using 13 variants of local binary patterns. *Pattern Recogn. Lett.* 68, 231–238.
- Huang, W., Yin, H., 2017. Robust face recognition with structural binary gradient patterns. *Pattern Recognit.* 68, 126–140.
- Hu, S., Pan, Z., Dong, J., Ren, X., 2022. A novel adaptively binarizing magnitude vector method in local binary pattern based framework for texture classification. *IEEE Signal Process. Lett.* 29, 852–856.
- Kabbai, L., Abdellaoui, M., Douik, A., 2019. Image classification by combining local and global features. *Visual Comput.* 35 (5), 679–693.
- Karanwal, S., Diwakar, M., 2021. OD-LBP: Orthogonal difference-local binary pattern for Face Recognition. *Digital Signal Process.* 110, 102948.
- Karczmarek, P., Kiersztyn, A., Pedrycz, W., Dolecki, M., 2017. An application of chain code-based local descriptor and its extension to face recognition. *Pattern Recognit.* 65, 26–34.
- Kas, M., Ruichek, Y., Messoussi, R., 2018. Mixed neighborhood topology cross decoded patterns for image-based face recognition. *Expert Syst. Appl.* 114, 119–142.
- Kas, Mohamed, Ruichek, Y., Messoussi, R., 2020. Multi level directional cross binary patterns: new handcrafted descriptor for SVM-based texture classification. *Eng. Appl. Artif. Intell.* 94, 103743.
- Lan, R., Lu, H., Zhou, Y., Liu, Z., Luo, X., 2019. An LBP encoding scheme jointly using quaternionic representation and angular information. *Neural Comput. Appl.*, 1–7.
- Li, L., Xia, Z., Wu, J., Yang, L., Han, H., 2022. Face presentation attack detection based on optical flow and texture analysis. *J. King Saud Univ.-Comput. Informat. Sci.* 34 (4), 1455–1467.
- Liu, L., Fieguth, P., Guo, Y., Wang, X., Pietikäinen, M., 2017. Local binary features for texture classification: Taxonomy and experimental study. *Pattern Recogn.* 62, 135–160.
- Liu, L., Chen, J., Fieguth, P., Zhao, G., Chellappa, R., Pietikainen, M., 2019. From BoW to CNN: Two decades of texture representation for texture classification. *Int. J. Comput. Vision* 127 (1), 74–109.
- Liu, J., Chen, Y., Sun, S., 2019. A novel local texture feature extraction method called multi-direction local binary pattern. *Multimedia Tools Appl.* 78 (13), 18735–18750.
- Luo, Q., Su, J., Yang, C., Silven, O., Liu, L., 2022. Scale-selective and noise-robust extended local binary pattern for texture classification. *Pattern Recogn.* 108901.
- Manjunath, B.S., Ma, W.Y., 1996. Texture features for browsing and retrieval of image data. *IEEE Trans. Pattern Anal. Machine Intell.* 18 (8), 837–842.
- Nanni, L., Lumini, A., Brahmam, S., 2010. Local binary patterns variants as texture descriptors for medical image analysis. *Artif. Intell. Med.* 49 (2), 117–125.
- Ojala, T., Pietikainen, M., Harwood, D., 1996. A comparative study of texture measures with classification based on feature distributions. *Pattern Recognit.* 29 (1), 51–59.
- Ouslimani, F., Ouslimani, A., Ameer, Z., 2019. Rotation-invariant features based on directional coding for texture classification. *Neural Comput. Appl.* 31 (10), 6393–6400.
- Pillai, A., Soundrapandian, R., Satapathy, S., Satapathy, S.C., Jung, K.H., Krishnan, R., 2018. Local diagonal extrema number pattern: a new feature descriptor for face recognition. *Future Generat. Comput. Syst.* 81, 297–306.
- Porter, R., Canagarajah, N., April, J., 1997. Robust rotation invariant texture classification. 1997 IEEE International Conference on Acoustics, Speech, and Signal Processing, vol. 4. IEEE, pp. 3157–3160.
- Rachdi, E., El merabet, Y., Akhtar, Z., Messoussi, R., 2020. Directional neighborhood topologies based multi-scale quinary pattern for texture classification. *IEEE Access* 8, 212233–212246.
- Roy, S.K., Chanda, B., Chaudhuri, B.B., Banerjee, S., Ghosh, D.K., Dubey, S.R., 2018. Local directional ZigZag pattern: A rotation invariant descriptor for texture classification. *Pattern Recogn. Lett.* 108, 23–30.
- Ruichek, Y., 2018. Local concave-and-convex micro-structure patterns for texture classification. *Pattern Recogn.* 76, 303–322.
- Ruichek, Y., 2019. Attractive-and-repulsive center-symmetric local binary patterns for texture classification. *Eng. Appl. Artif. Intell.* 78, 158–172.
- Shih, H.C., Cheng, H.Y., Fu, J.C., 2020. Image classification using synchronized rotation local ternary pattern. *IEEE Sens. J.* 20 (3), 1656–1663.
- Shu, Xin et al., 2022. Using global information to refine local patterns for texture representation and classification. *Pattern Recogn.* 131, 108843.
- Song, T., Li, H., Meng, F., Wu, Q., Cai, J., 2017. Letrist: locally encoded transform feature histogram for rotation-invariant texture classification. *IEEE Trans. Circuits Syst. Video Technol.*
- Song, T., Feng, J., Luo, L., Gao, C., Li, H., 2020. Robust texture description using local grouped order pattern and non-local binary pattern. *IEEE Trans. Circuits Syst. Video Technol.* 31 (1), 189–202.
- Song, T., Feng, J., Luo, L., Gao, C., Li, H., 2020. Robust texture description using local grouped order pattern and non-local binary pattern. *IEEE Trans. Circuits Syst. Video Technol.* 31 (1), 189–202.
- Song, T., Xin, L., Gao, C., Zhang, T., Huang, Y., 2021. Quaternionic extended local binary pattern with adaptive structural pyramid pooling for color image representation. *Pattern Recogn.* 115, 107891.
- Sucharitha, G., Senapati, R.K., 2019. Biomedical image retrieval by using local directional edge binary patterns and Zernike moments. *Multimedia Tools Appl.*, 1–18.
- Tan, X., Triggs, B., 2010. Enhanced local texture feature sets for face recognition under difficult lighting conditions. *IEEE Tran. Image Process.* 19 (6), 1635–1650.
- Tan, X.Y., Triggs, B., 2010. Enhanced local texture feature sets for face recognition under difficult lighting conditions. *IEEE Trans. Image Process.* 19 (6), 1635–1650.
- Torrallba, A., Fergus, R., Freeman, W.T., 2008. 80 million tiny images: A large data set for nonparametric object and scene recognition. *IEEE Trans. Pattern Anal. Mach. Intell.* 30 (11), 1958–1970.
- Tuncer, T., Dogan, S., 2020. Pyramid and multi kernel based local binary pattern for texture recognition. *J. Ambient Intell. Humanized Comput.* 11 (3), 1241–1252.
- Varma, M., Zisserman, A., 2008. A statistical approach to material classification using image patch exemplars. *IEEE Trans. Pattern Anal. Mach. Intell.* 31 (11), 2032–2047.
- Xu, Y., Yang, X., Ling, H., Ji, H., 2010. A new texture descriptor using multifractal analysis in multi-orientation wavelet pyramid. In: 2010 IEEE Computer Society Conference on Computer Vision and Pattern Recognition. IEEE, pp. 161–168.
- Yang, W., Zhang, X., Li, J., 2020. A local multiple patterns feature descriptor for face recognition. *Neurocomputing* 373, 109–122.
- Zheng, C.H., Pei, W.J., Yan, Q., Chong, Y.W., 2017. Pedestrian detection based on gradient and texture feature integration. *Neurocomputing* 228, 71–78.
- Zheng, Z., Xu, B., Ju, J., Guo, Z., You, C., Lei, Q., Zhang, Q., 2022. Circumferential local ternary pattern: new and efficient feature descriptors for anti-counterfeiting pattern identification. *IEEE Trans. Inf. Forensics Secur.* 17, 970–981.